

Growth and property characterizations of photonic crystal structures consisting of colloidal microparticles

Hong-Bo Sun* and Junfeng Song

Department of Electronic Engineering, Jilin University, 119 Jiefang Road, Changchun 130023, China

Ying Xu, Shigeki Matsuo, and Hiroaki Misawa[†]

Department of Ecosystem Engineering, Graduate School of Engineering, Satellite Venture Business Laboratory, The University of Tokushima, 2-1 Minamijosanjima, Tokushima 770-8506, Japan

Guotong Du and Shiyong Liu

State Key Laboratory on Integrated Optoelectronics, Jilin University, 119 Jiefang Road, Changchun 130023, China

Received July 15, 1999; revised manuscript received October 26, 1999

High-quality three-dimensional polystyrene–air photonic crystal structures with particle diameters of 200, 270, and 340 nm were grown with a quasi-equilibrium evaporation technique. The effects of the removal of interval water were evident as a blueshift of peaks, enhancement of the transmission attenuation, and changes in the gap/midgap ratio. Frequency scaling and incidence-angle-dependent transmission were also investigated; both show good agreement with the numerical simulation. © 2000 Optical Society of America [S0740-3224(00)01103-6]

OCIS codes: 290.5850, 310.2790, 310.6860, 160.4670, 160.4760, 160.4890.

1. INTRODUCTION

Colloidal dispersions have attracted considerable attention as the result of their rich thermodynamic properties^{1,2} and their industrial and medical utility. A new application of colloidal crystals in which there is significant long-range spatial order is their photonic bandgap effects.^{3,4} A system of three-dimensionally periodically arrayed particles offers a natural way to tailor the colloidal crystal's internal electromagnetic modes into a bandgap structure in which propagation of electromagnetic waves is forbidden irrespective of direction.^{5,6} Now photonic crystals have not only attracted extensive research interest in the interaction of light and matter, such as light localization, but have also exhibited prospects for wide application, for example, in extremely low-threshold lasers, integrated optical microwaveguides, and filters.^{3–8}

Some techniques were recently proposed and employed for the fabrication of such spatially periodic dielectric structures, including mechanical drilling,⁷ self-assembling of colloidal particles,^{3,4,8} wet and dry etching,^{9,10} film deposition,¹¹ photopolymerization of resin,¹² and laser microexplosion in transparent dielectrics.¹³ Despite the rapid progress in this field, the self-assembly of colloidal particles is still desirable because it would provide ease of fabrication, a high degree of ordering in three dimensions, a wide range of variations of bandgap peak positions (from the visible to the infrared and the microwave region, depending on the particle sizes), and suitability for large-area samples.

The dielectric contrast (β , the ratio of the refractive indices n of the component materials) is analogous to the depth of a potential well in generic electronic crystals.⁶ Typically, increasing β pronouncedly enhances photonic bandgap effects. This was conveniently achieved by the removal of the solvent (water, $n_{\text{water}} \approx 1.3$, for polystyrene microsphere aqueous colloids in the current research), which left air ($n_{\text{air}} \approx 1.0$) in particle intervals.⁸ However, a high density of crystal defects (point defects, such as vacancies; line defects, such as dislocations; and volume defects, such as stacking faults and heteroboundaries) is liable to occur in this process owing to forced sedimentation. In other words, the water typically evaporates too fast at room temperature and room humidity (e.g., relative humidity RH \sim 40%) than is necessary for particles to settle, because the ratio of cell side length to cell depth is typically very large (for example, 10 mm/0.2 mm = 50 in this research; see below for details). The particle “atoms” have no time to relax to their normal lattice sites. In Ref. 8 some of us proposed a quasi-equilibrium sedimentation technique in which the sample was settled under high RH to suppress the evaporation of water (supernatant and interval). In this paper we report a similar technique used to fabricate samples (improved in two aspects introduced in Section 2) and make a systematic investigation of the crystal properties.

2. EXPERIMENTAL PROCEDURE

The samples were prepared from a stock of polystyrene solution of known particle concentration, with the volume

fraction $\phi_0 \sim 0.05$. The particles have mean radii of approximately 200, 270, and 340 nm and a polydispersity [(standard deviation of the particle size distribution)/mean] of ≤ 0.05 . They were concentrated by low-speed centrifugation to form a dense sediment, followed by removal of a weighed amount of clear supernatant liquid. Slow tumbling of the samples with ion exchange resin then redispersed particles effectively, left them positionally randomized (showing only local short-range order). The fractional volume ϕ of the samples occupied by polystyrene particles was calculated from the initial concentration value ϕ_0 and the volume of removed water. Suspensions of various particle concentrations were sustained in a square cell with an area of $10 \text{ mm} \times 10 \text{ mm}$ and a depth of $200 \mu\text{m}$. The cell was carved out of a silica plate, which was partly protected by HF-proof adhesive tape, by immersion of the plate in 5% hydrofluoric acid for 24 h at room temperature. The samples were kept undisturbed in a thermostatic chamber in which the humidity can be continuously adjusted with an accuracy of approximately $\pm 5\%$. During particle sedimentation (~ 1 week) the RH was kept high and constant. When the process was complete, the RH was gradually decreased to room humidity (for ~ 50 h) so that the supernatant and interval water was evaporated without distorting the lattices. This possibility offers us a more reliable and effective control of the evaporation rates than in Ref. 8, where the RH was controlled at fixed levels of 30% and 90%.

For the transmission measurements, the beam of a xenon lamp was collimated, slightly focused, and passed through a rectangular aperture so that a surface area of the sample of $\sim 1 \text{ mm}^2$ was illuminated. Parallely transmitted light was focused onto a vertical slit, which preceded a diffuser and a photomultiplier-tube detector.

3. RESULTS AND DISCUSSION

A. Growth of Colloidal Crystal

The nominally simple sedimentation process actually combines gravity settling, diffusion, and crystallization.¹⁴ For the growth of crystals the balance between diffusion and sedimentation is important. This balance is described by the Peclet number, Pe , which is defined as the ratio of the time that it takes a particle to diffuse over a distance R and the time that it takes for a particle to settle over the same distance. $Pe = m_B g R / k T$, where m_B is the buoyant mass of a particle with radius R and g is the gravitational acceleration. In this investigation, Pe is 112, 375, and 943 for particle diameters of 200, 270, and 340 nm, respectively. As Pe increases, the tendency of particles to be deposited increases compared with their tendency to diffuse. However, microsphere "atoms" still have sufficient time to shift to low-potential sites. Judging by the results of transmission measurements (see Fig. 3 below), the crystal quality was increased for higher Peclet numbers.

Apparently there should be some limitation to particle sizes for the diffusion–sedimentation–crystallization balance. Also, supernatant water evaporation that is too fast inevitably spoils the balance, ultimately leading to a

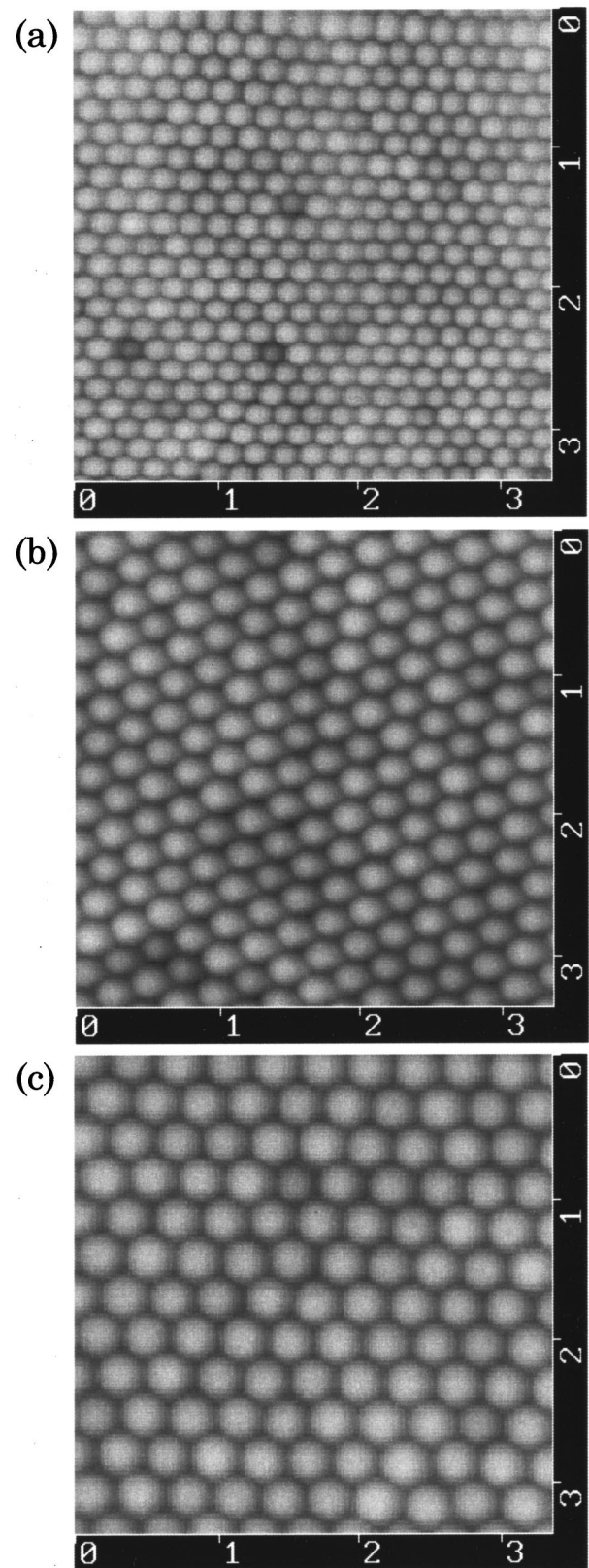


Fig. 1. Atomic-force microscope images of surfaces of colloidal-particle photonic crystal structures fabricated with a quasi-equilibrium evaporation process. A high crystal quality was achieved by control of the evaporation of supernatant and interval water. The microsphere diameters are (a) 200, (b) 270, and (c) 340 nm. For all samples the thickness was 50 layers, corresponding to a lattice periodicity of approximately 17.

disordered state if the rate of sedimentation is higher than that for crystallization. RH under this circumstance was therefore kept at approximately 90% during particle deposition, after which it was gradually decreased to room humidity. The gradually changed RH helps the particles overcome surface tension, which is especially important for achieving a high crystal quality in surface layers. Figure 1 shows atomic-force microscopic images of surfaces of three different samples fabricated by the present techniques. The thicknesses of the samples were chosen to be 50 layers, corresponding to an approximately 17-period lattice in the $\langle 111 \rangle$ close-packing direction.

The microspheres have a permanent negative net surface charge counterbalanced by free ions in the solution. Once the free ions are removed with an ion-exchange resin, the microspheres interact with a short-range repulsive Coulomb force in addition to a long-range attractive van der Waals force. As a result of this interaction, face-centered-cubic (fcc) packing was favored in the crystallization.^{4,15} This is another point of improvement compared with Ref. 8, in which hexagonal close packing (hcp) cannot be excluded. Once the crystallization is complete, the particle motions are largely limited to local Brownian excursions centered on sites in the regular crystalline array.

B. Characterization of Bandgap Effect

Three factors influence photonic bandgap effects, namely, lattice type, filling ratio, and dielectric contrast. Our crystals are fcc structures in which there is only a narrow bandgap at the eighth and ninth bands; a pseudogap between the second and third bands⁶ is used here for characterization of structural properties. The filling ratio of the dielectric for close-packing ball lattices is always 0.74, and the contrast of refractive indices is $\beta = 1.6$ (polystyrene/air).

To confirm whether the internal water had evaporated, transmission spectra were taken before and after evaporation of the same sample when the sedimentation was complete, as is shown in Fig. 2. The weak bandgap effect (small gap/mid-gap ratio of 0.017 before compared with 0.089 after and small bandgap rejection of -8 dB before compared with -17 dB after) indicated by the transmission valley (or Bragg notch) profile at 660 nm are both naturally attributed to the smaller dielectric contrast between polystyrene and water (1.22). The notch-center shift of 35 nm (from 660 to 625 nm) offers direct evidence⁸ for the elimination of water, because the refractive index of the polystyrene-air composite (1.46) is smaller than that for polystyrene-water (1.53). The evaporation does not degrade the crystal quality, and the much stronger bandgap effects can be explained only by the increased dielectric contrast.

One important feature of a photonic bandgap compared with an electronic crystal is its scaling property.¹⁶ In an atomic system the potentials have the fundamental length scale of the Bohr radius, so that configurations differing only in their absolute length scale nevertheless have very different behaviors. The photonic bandgap is described by the following equation (master equation, obtained from Maxwell's equation¹⁶):

$$\nabla \times \left[\frac{1}{\epsilon(\mathbf{r})} \nabla \times \mathbf{H}(\mathbf{r}) \right] = \left(\frac{\omega}{c} \right)^2 \mathbf{H}(\mathbf{r}), \quad (1)$$

where ω and c are the mode frequency and the speed of light in vacuum, respectively; the lattice periodicity is reflected by the spatial distribution of dielectric constant, $\epsilon(\mathbf{r})$. It is easy to deduce from Eq. (1) that changing the length scale by some factor causes the corresponding mode and frequency to be scaled by the same factor. These relationships were evident from the measured and the calculated size-dependent transmission valley wavelengths. Corresponding to different particle diameters of 200, 270, and 340 nm, transmission valleys occur at 464, 625, and 805 nm [Fig. 3(a)]. The spectra agree with those from numerical calculations (dashed curves).

For the transmission simulation we used a transfer matrix technique that defines how waves cross a slab of materials and is therefore closely related to the transmission and reflection coefficients. If the electronic and the magnetic fields in the x - y plane at $z = 0$ are known, Maxwell's equation can be used as a fixed frequency to integrate the electronic and the magnetic fields in the x - y plane at $z = c$. If both the electric displacement field, \mathbf{D} , and the magnetic induction field, \mathbf{B} , are assumed to have zero divergence, we need to know only two components of each field:

$$\mathbf{F}(z = 0) = [E_x(z = 0), E_y(z = 0), H_x(z = 0), H_y(z = 0)]. \quad (2)$$

Then the transfer matrix is defined by

$$\mathbf{F}(z = c) = \mathbf{T}(c, 0)\mathbf{F}(z = 0). \quad (3)$$

If the lattice periodicity of the crystal is sufficiently high, the Bloch condition can be imposed to allow us to calculate the band structure. Numerical solution of the above procedure requires Maxwell's equations to be reformulated on a lattice,^{17,18} and the algorithms used for construction of \mathbf{T} were quite similar to those of Bell *et al.*¹⁹

The particle-diameter-dependent bandgap center wavelengths are plotted in Fig. 3(b). The data for the 220-nm particle are from Ref. 8. The strongest attenua-

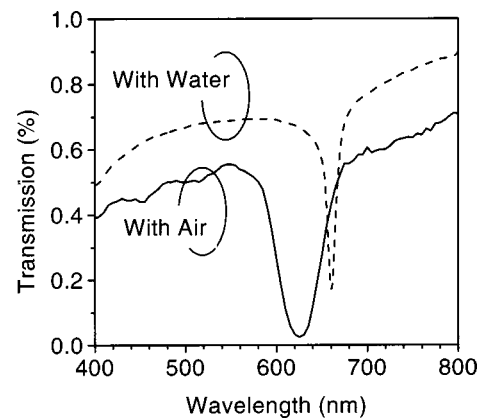


Fig. 2. Normalized transmission spectra of colloidal crystal structures (solid curve) before and (dashed curve) after the removal of water. To avoid disturbances in transportation, the sample was fixed in the light path beforehand; the experimental configuration was specially designed to permit this. A gradual variation of spectra from the solid to the dashed curve was observable.

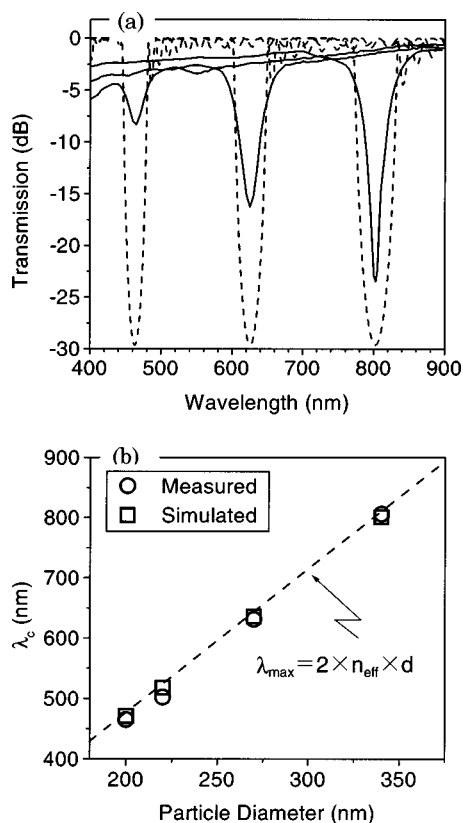


Fig. 3. Microsphere diameter-dependent transmission properties. (a) The leftmost, central, and rightmost spectral valleys correspond to particle diameters of $2r$ of 200, 270, and 340 nm, respectively. The solid curves are from measurements and the dashed curves from the simulation. (b) A comparison of measured and theoretical central wavelengths of transmission valleys of fcc photonic crystal structures. The open circles and open squares are from measurement and from numerical calculation by plane-wave expansion technique, respectively. The guiding dashed line is drawn according to Bragg's law.

tion, -25 dB, was achieved with the 350-nm sample, which implies a higher crystal quality than in the other two (-8 and -17 dB for the 200- and the 270-nm samples, respectively).

Transmission measurements were also performed at various incidence angles (α) with respect to the surface normal. To illustrate the experimental strategy, the first Brillouin zone (FBZ) with the principal symmetry points for the fcc crystal is shown in Fig. 4(a). Normalized transmission along the $L \rightarrow W$ direction was measured for the crystal packed with 270-nm particles, as is shown in Figs. 4(b) and 4(c). At normal incidence ($\alpha = 0$) a clear attenuation was observed at 625 nm [Fig. 3(a)]. As the angle increased ($\alpha = 0 \sim 40^\circ$), the bandgap blue-shifted to a shorter wavelength according to Bragg's law. The accuracy of the angle measurement is within $\pm 2^\circ$, and all three samples exhibit similar behavior. The dashed line of Fig. 3(b) is from a calculation, and the circles are measured data. Moving the light propagation from point L ($L + 0^\circ$) along $L \rightarrow W$ ($L + 51.1^\circ$) to ($L + 40^\circ$) decreased the center wavelength by a total of ~ 130 nm. This can be understood by considering that plane waves sense a decreased periodicity (increased wave vector) from points L to W because point L is closer to the center of FBZ and point W is the farther.

What is noteworthy is the influence of surface cracking. The entire 1-mm^2 detecting area consists of hundreds of domains pronouncedly demarcated by crevices. A typical profile of a 270-nm sample taken across a domain boundary is shown in Fig. 5. A single domain area averages $5 \times 10^3 \mu\text{m}^2$. However, the transmission was not degraded by the existence of multiple domains, which was proved by reduction of the detection area to $50 \times 50 \mu\text{m}^2$, a region without any visible surface defects. This outcome implies that the domains were made up of single bulk crystals. The large-area transmission was the sum of that from parallel single crystals. This held true until the surface defect density became very high (e.g., $>0.05 \mu\text{m}^{-2}$, all deduced to be equivalent to point defects) and except for single-crystal regions of less than several tens of square micrometers.

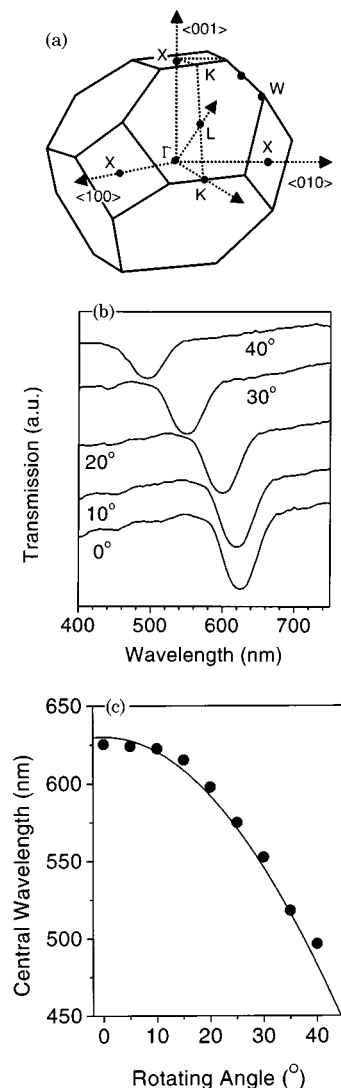


Fig. 4. Incidence-angle-dependent bandgap effects (the microsphere diameter is $2r = 270$ nm). (a) The FBZ of fcc photonic lattices. The principal symmetry points (Γ , L, K, W, and X) and axes are illustrated. (b) Transmission spectra, measured along the $L \rightarrow W$ direction at various positions: $L + 0^\circ$, $L + 10^\circ$, $L + 20^\circ$, $L + 30^\circ$, and $L + 40^\circ$. (c) Incidence-angle-dependent wavelength of transmission valley centers. The curve is from Bragg's law, and filled circles are abstracted from (b).

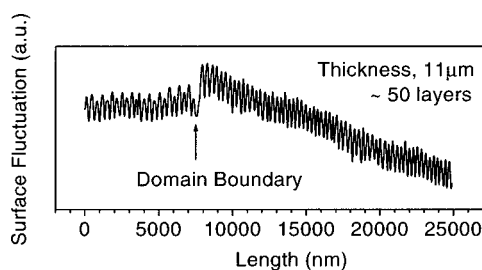


Fig. 5. Surface profile of a colloidal crystal consisting of multiple single-crystal domains. The cross section was chosen to cross the boundary of two single-crystal regions. Judging from the peaks' spacing and height variation, the measured zone contains two single-crystal domains with different orientations.

4. CONCLUSION

High-quality photonic crystal structures have been achieved by the self-organization of colloidal particles with a quasi-equilibrium evaporation technique. The effects of the removal of background water were seen as a 35-nm blueshift of the peak position, a fivefold increase of the gap/midgap ration, and a -9 -dB larger transmission attenuation. The transmission valley scales linearly with particle size; e.g., central wavelengths were at 464, 625, and 805 nm for microsphere diameters of 200, 270, and 340 nm, respectively. The dependence of the central wavelength valley on the incidence angle is interpreted as variations of wave vectors in the FBZ. Finally, we observed that the bandgap effect is not degraded by the existence of polycrystalline states only when the single-crystal domain is sufficiently large compared with the lattice constant.

ACKNOWLEDGMENT

The current work was supported in part by the China Natural Science Foundation, the Satellite Venture Business Laboratory of The University of Tokushima, and the Marubun Research Promotion Foundation.

*Present address, Satellite Venture Business Laboratory, The University of Tokushima, 2-1 Minamijyosan-jima, Tokushima 770-8506, Japan; e-mail, hbsun@ieee.org.

†Corresponding author: misawa@eco.tokushima-u.ac.jp.

REFERENCES

1. A. Vrij, "Polymers at interfaces and the interactions in colloidal dispersions," *Pure Appl. Chem.* **48**, 471–483 (1976).
2. A. D. Dinsmore, A. G. Yodh, and D. J. Pine, "Phase diagrams of nearly hard-sphere binary colloids," *Phys. Rev. E* **52**, 4045–4057 (1995).
3. R. Biswas, M. M. Sigalas, G. Subramania, and K.-M. Ho, "Photonic band gaps in colloidal systems," *Phys. Rev. B* **57**, 3701–3705 (1998).
4. I. Tarhan and G. H. Watson, "Photonic band structure of fcc colloidal crystals," *Phys. Rev. Lett.* **76**, 315–318 (1996).
5. E. Yablonovitch, "Inhibited spontaneous emission in solid-state physics and electronics," *Phys. Rev. Lett.* **58**, 2059–2063 (1987).
6. For a review, see, for example, articles in C. Soukoulis, ed., *Photonic Band Gap Materials*, Vol. 315 of NATO ASI Series E (Kluwer, Dordrecht, 1996).
7. E. Yablonovitch and T. G. Gmitter, "Photonic band structure: the face-centered cubic case," *Phys. Rev. Lett.* **63**, 1950–1953 (1989).
8. K. Fukuda, H. Sun, S. Matsuo, and H. Misawa, "Self-organizing three-dimensional colloidal photonic crystal structure with augmented dielectric contrast," *Jpn. J. Appl. Phys.*, **37**, L508–L511 (1998).
9. S. Y. Lin, J. G. Fleming, D. L. Hetherington, B. K. Smith, Y. Biswas, K. M. Ho, M. M. Sigalas, W. Zubrzycki, S. R. Kurtz, and J. Bur, "Three-dimensional photonic crystal operating at infrared wavelengths," *Nature* **394**, 251–253 (1998).
10. U. Grüning, V. Lehmann, and C. M. Engelhardt, "Two-dimensional infrared photonic band gap structure based on porous silicon," *Appl. Phys. Lett.* **66**, 3254–3256 (1995).
11. O. Hanaizumi, Y. Ohtera, T. Sato, and H. Kawakami, "Propagation of light beams along line defects formed in α -Si/SiO₂ three-dimensional photonic crystals: fabrication and observation," *Appl. Phys. Lett.* **74**, 777–779 (1999).
12. H.-B. Sun, S. Matsuo, and H. Misawa, "Three-dimensional photonic crystal structures achieved with two-photon-absorption photopolymerization of resin," *Appl. Phys. Lett.* **74**, 786–788 (1999).
13. H.-B. Sun, Y. Xu, S. Matsuo, and H. Misawa, "Microfabrication and characteristics of two-dimensional photonic crystal structures in vitreous silica," *Opt. Rev.* **6**, 396–398 (1999).
14. P. N. Pusey and W. V. Megen, "Phase behavior of concentrated suspensions of nearly hard colloidal spheres," *Nature* **320**, 340–342 (1986).
15. P. Pieranski, "Colloidal crystals," *Contemp. Phys.* **24**, 25–73 (1983).
16. J. Joannopoulos, R. Meade, and J. Winn, *Photonic Crystals* (Princeton U. Press, Princeton, N.J., 1995).
17. See T. K. Gaylord, G. N. Henderson, and E. N. Glytsis, "Application of electromagnetic formalism to quantum-mechanical electron-wave propagation in semiconductors," *J. Opt. Soc. Am. B* **10**, 333–339 (1993).
18. J. B. Pendry, "Photonic band structures," *J. Mod. Opt.* **41**, 209–229 (1993).
19. P. M. Bell, J. B. Pendry, L. Martín-Moreno, and A. J. Ward, "A program for calculating photonic band structures and transmission coefficient of complex structures," *Comput. Phys. Commun.* **85**, 306 (1995).